

Propagation of Intersheath Modes on Underground Cables

I. Lafaia, Y. Yamamoto, A. Ametani, J. Mahseredjian, M. T. Correia de Barros, I. Koçar, A. Naud

Abstract — This paper investigates wave propagation and transients associated with intersheath modes on normal-bonded and cross-bonded underground cables. Circuits for exciting intersheath modes are analyzed based on simulation and propagation characteristics of a cable system. It is observed that if the source is grounded, several modal components will be overlapped. Also when a purely intersheath mode wave travels in a cross-bonded cable the reflections and refractions occurring at each crossbonding point produce additional modes of propagation. A homogeneous model for long cross-bonded cables allows the computation of modal characteristics of the system facilitating its analysis and it presents advantages in terms of simulation time. The accuracy of the homogeneous model and the advantage of its use is greater as the length of the system and the number of sheath grounding points increases.

Keywords: *underground cable, normal-bonded cable, cross-bonded cable, wave propagation, electromagnetic transients, intersheath modes, EMTP, homogeneous model.*

I. INTRODUCTION

Recently, a number of high voltage cable projects have been proposed all over the world and some of them are currently under construction. This is mainly due to the installation of off-shore wind farms, the use of high voltage AC cables for grid development, and partially due to human safety requirements against electrostatic and electromagnetic hazards caused by overhead transmission lines [1]. For example, a 400kV AC submarine cable connecting Italian mainland and Sicily Island is under construction [2]. The Boute-Trans project of the French Transmission System Operator (Réseau de Transport d'Électricité) involves the installation of a 66 km long 225 kV AC cable in the south east of France. In Denmark, all the 132kV to 150kV overhead transmission lines are planned to be undergrounded by the year of 2040 [3].

There are many papers investigating wave propagation and transient characteristics of cables [1, 4-19]. Most of these papers are concerned with coaxial mode wave propagation and transients. Only few papers investigated wave propagation and transient characteristics due to the earth-return and

intersheath modes, i.e. propagation between metallic sheaths including earth [1, 12, 18].

References [1, 18] discussed the significance of a transient due to an intersheath mode based on a field measurement. The both ends of the metallic sheaths were open-circuited in the field test. Since in practice, all the sheaths are grounded at every major section, it is not clear if the measured result is applicable to the case of a real cable.

This paper investigates wave propagation characteristics of intersheath modes and resultant transient voltages and currents on underground cables with normal-bonding and cross-bonding. The circuits recommended for intersheath mode excitation in field tests are first analyzed and explained based on EMTP simulations and on the propagation characteristics of the system. The effect of grounding a source in a field test is also explained. A so-called homogeneous model for cross-bonded cables is also explained and its accuracy is tested with simulation of electromagnetic transients (EMT) in EMTP.

II. THEORETICAL ANALYSIS OF INTERSHEATH MODES

A. Intersheath modes

Wave propagation on a multi-phase conductor is characterized by the modal propagation constant γ and the voltage and current transformation matrices \mathbf{A} and \mathbf{B} . In the case of a three-phase single core coaxial (SC) cable composed of a core conductor and a metallic sheath, the transformation matrices are given approximately in the following form in the high frequency region, i.e. for a transient analysis [14]. Bold characters are used to denote vectors and matrices hereinafter.

$$\mathbf{V}_m = \mathbf{A}^{-1} \mathbf{V}_{ph}, \quad \mathbf{A}^{-1} = \begin{bmatrix} \mathbf{0} & \mathbf{a} \\ \mathbf{U}' & -\mathbf{U}' \end{bmatrix} \quad (1)$$

$$\mathbf{a} = \frac{1}{3} \begin{bmatrix} 1 & 1 & 1 \\ -1 & 2 & -1 \\ -3/2 & 0 & 3/2 \end{bmatrix}, \quad \mathbf{U}' = \begin{bmatrix} 0 & 0 & 1 \\ 1 & 0 & 0 \\ 0 & 1 & 0 \end{bmatrix} \quad (2)$$

$$\mathbf{V}_m = [V_0 \ V_1 \ V_2 \ V_3 \ V_4 \ V_5]^T \quad (3)$$

$$\mathbf{V}_{ph} = [V_{ca} \ V_{cb} \ V_{cc} \ V_{sa} \ V_{sb} \ V_{sc}]^T$$

In (3), subscript 'c' is used for core-to-ground voltage and subscript 's' is used for sheath-to-ground voltage. Subscripts 'a', 'b', and 'c' identify each phase and numbers 0 to 5 identify the modes. It is observed in (1) to (3) that modes 0, 1 and 2 depend only on sheath voltages V_{sa} , V_{sb} , and V_{sc} . It is also observed that $V_0 = (V_{sa} + V_{sb} + V_{sc})/3$ is a 0-sequence (or earth-return) voltage, whereas modes 1 and 2 are intersheath modes. From these observations and because this paper is focused on intersheath mode propagation, we can simplify equation (1) by eliminating core voltages:

A. Ametani, I. Lafaia, J. Mahseredjian, I. Koçar are with Polytechnique Montreal, 2500, chemin de Polytechnique, Montréal (Québec) H3T1J4, Canada (e-mail: isabel.lafaia@polymtl.ca).

Y. Yamamoto is with Doshisha University, Karasuma-higashi-iru, Imadegawa-dori, Kamigyo-ku, Kyoto-shi 602-8580, Japan.

M. T. Correia de Barros is with Instituto Superior Técnico, Universidade de Lisboa, Avenida Rovisco Pais 1, 1049-001 Lisboa, Portugal. A. Naud is with Réseau de Transport d'Électricité, Cœur Défence-100 esplanade du Général de Gaulle, 92932 Paris La Défense Codex, France.

$$\mathbf{V}_e = (\mathbf{A}')^{-1} \mathbf{V}_s, (\mathbf{A}')^{-1} = \mathbf{a} \quad (4)$$

Where $\mathbf{V}_e = [V_0 \ V_1 \ V_2]^T$ and $\mathbf{V}_s = [V_{sa} \ V_{sb} \ V_{sc}]^T$ are sub-vectors of \mathbf{V}_m and \mathbf{V}_{ph} , respectively. In a similar way for currents

$$\mathbf{I}_e = (\mathbf{B}')^{-1} \mathbf{I}_s, (\mathbf{B}')^{-1} = (\mathbf{A}')^T = \begin{bmatrix} 1 & 1 & 1 \\ -1/2 & 1 & -1/2 \\ -1 & 0 & 1 \end{bmatrix} \quad (5)$$

where $\mathbf{I}_e = [I_0 \ I_1 \ I_2]^T$ and $\mathbf{I}_s = [I_{sa} \ I_{sb} \ I_{sc}]^T$.

B. Circuits for intersheath modes

Fig. 1 illustrates intersheath mode circuits corresponding to the transformation matrix in (2). Considering the circuit in Fig. 1(a), if we assume that the 3 phases are absolutely symmetrical (approximation validated in Chapter III.A), then the source will inject a current that will return half in each of the adjacent phases, that is

$$I_{sa} = -I/2, I_{sb} = I, I_{sc} = -I/2 \quad (1)$$

By combining (5) and (6), the modal currents become

$$I_0 = 0, I_1 = 3I/2, I_2 = 0 \quad (2)$$

This result shows that only mode 1 (first intersheath mode) exists in the circuit of Fig. 1(a).

In Fig. 1(b) the currents at the sending end are given by

$$I_{sa} = I, I_{sb} = 0, I_{sc} = -I \quad (3)$$

By combining (5) and (8), the modal currents become

$$I_0 = 0, I_1 = 0, I_2 = -2I \quad (4)$$

The above equation clearly shows that only mode 2 (second intersheath mode) current exists in the circuit in Fig. 1(b).

It is common in a field test to ground the source to avoid dangerous voltages in accessible terminals. When the voltage source in the circuits of Fig. 1 is grounded, the sum of the three-phase sheath currents is not zero and from (5) it is observed that $I_0 = I_{sa} + I_{sb} + I_{sc} = I_g \neq 0$. In such a case, an earth-return mode will be superposed to the intersheath modes observed in the circuits of Fig. 1.

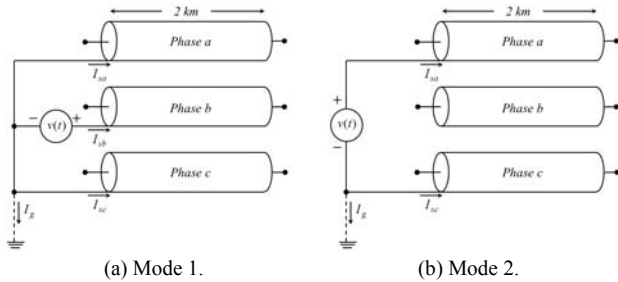


Fig. 1. Circuits for energization of modes 1 and 2 (intersheath modes) corresponding to the transformation matrix in (2). If the source is grounded, an earth-return mode is excited.

C. Modal Attenuation and Velocity

Fig. 2 illustrates the cross-section and the arrangement of a three-phase XLPE cable. Fig. 3 shows the modal attenuation and velocity of the system in Fig. 2. The earth-return mode (mode 0) is substantially different from the other modes for any frequency above 100 Hz. Attenuation of intersheath modes 1 and 2 and coaxial modes 3 to 5 is not very different. However, intersheath modes have propagation velocities

substantially lower than coaxial modes, and thus it appears possible to observe the effect of the intersheath modes on transient voltages and currents from a difference of traveling time of the modal components [14]. Table I gives values of modal attenuation and velocity at 50 kHz which are used for analyzing simulation results in Chapter III.

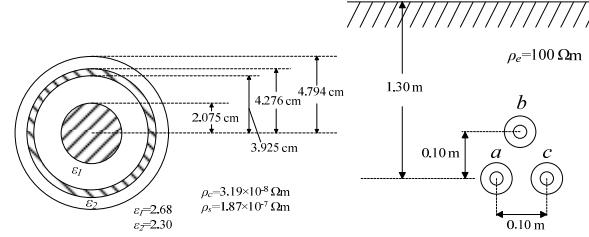
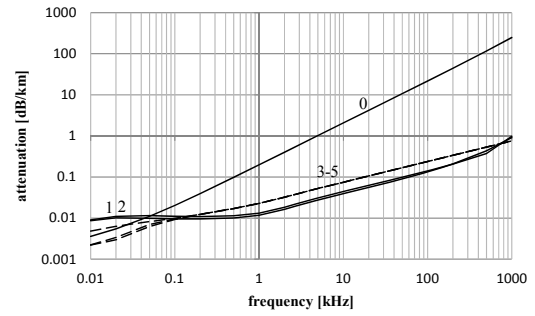
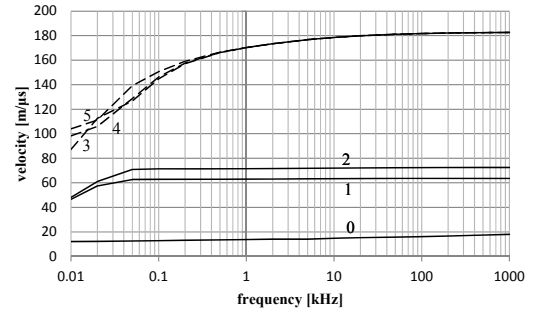


Fig. 2. Underground three-phase XLPE cable.



a) Modal attenuation.



b) Modal velocity.

Fig. 3. Modal frequency responses of the normal-bonded cable in Fig. 2.

TABLE I.
CABLE CONSTANTS AT F=50 KHZ – MODAL COMPONENTS

Mode no.	0	1	2	3	4,5
Attenuation [dB/km]	10.71	0.11	0.17	0.25	0.17
Velocity [m/us]	15.78	63.54	72.19	180.04	181.07

III. SIMULATED INTERSHEATH MODE WAVEFORMS

This chapter presents simulation results of the circuits in Fig. 1 using the cable system in Fig. 2. A 1.2 μ s/50 μ s impulse voltage with the amplitude of 2 kV is applied at the sending end. The simulations are carried out in EMTP-RV [20] using a wideband cable model. The excitation of first and second intersheath modes is presented in Sections III.A and III.B. The effect of grounding the source in the circuit of Fig. 1(b) is analyzed in Section III.C.

A. First intersheath mode

Fig. 4 shows the phase-a receiving end sheath voltage in the circuit in Fig. 1(a). The oscillating period T is about $126 \mu\text{s}$. Since the cable is open-circuited, this corresponds to four times the traveling time τ along the cable. Thus, the propagation delay and the velocity are calculated as $\tau = T/4 = 31.5 \mu\text{s}$ and $c = 2000/31.5 = 63 \text{ m}/\mu\text{s}$. This velocity agrees with the first intersheath mode (mode 1) in Table I. Fig. 5, presenting modal voltages calculated from the simulated results at the receiving end of the circuit in Fig. 1(a), further confirms this observation by showing that mode-0 and mode-2 voltages are nearly zero compared to mode-1 voltage. Thus, it is clear that only the first intersheath mode (mode 1) is generated in the circuit in Fig. 1(a).

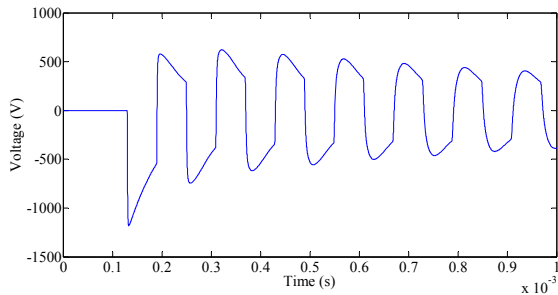


Fig. 4. Simulated sheath-a receiving end voltage in the circuit of Fig. 1(a).

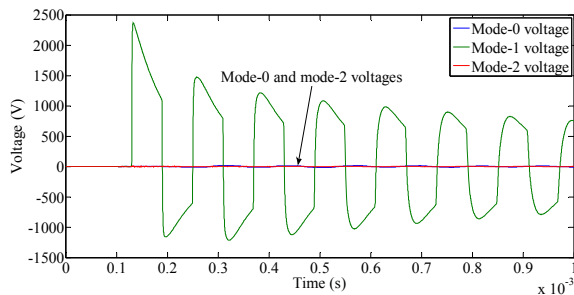


Fig. 5. Mode-0, mode-1, and mode-2 voltages calculated from simulation results of voltages at the receiving end of the circuit in Fig. 1(a).

B. Second intersheath mode

Fig. 6 shows the phase-a receiving end sheath voltage observed in the circuit of Fig. 1(b) using the cable design in Fig. 2. The oscillating period is $T = 110 \mu\text{s}$. The propagation delay and velocity are $\tau = T/4 = 27.5 \mu\text{s}$ and $c = 2000/27.5 = 72.7 \text{ m}/\mu\text{s}$, which agrees with the second intersheath mode (mode 2) in Table I. Fig. 7, presenting the voltages of modes 0, 1, and 2 at the receiving end of the circuit in Fig. 1(b), further confirms that only the second intersheath mode is excited in the circuit of Fig. 1(b).

C. Grounded voltage source

In a field test, it is a usual practice to ground the source to avoid dangerous voltages at accessible terminals. This case is investigated in Fig. 8, showing EMTP simulation results of receiving end voltage of sheath-a when the source in Fig. 1(b) is grounded. Contrary to Fig. 6, for ungrounded source, the voltage in Fig. 7 shows that besides the main oscillating frequency there is another harmonic of lower frequency and some spikes are noticed at certain points. The modes at the

receiving end of the circuit in Fig. 1(b) are plotted in Fig. 9. By comparing Figs. 7 and 9 it is observed that when the source in Fig. 1(b) is grounded mode-0, mode-1 and mode-2 will be superimposed whereas when the source is isolated from the ground, only mode-2 is present. As expected, it is easy to observe in Fig. 9 that the mode-0 has the lowest velocity whereas mode-1 has a voltage slightly lower than mode-2, which agrees with the values in Table I.

Thus, it is concluded that it is difficult to measure only an intersheath mode in a field test with a source grounded.

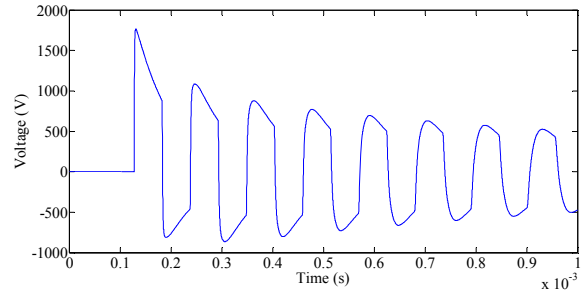


Fig. 6. Simulated sheath-a receiving end voltage in the circuit of Fig. 1(b).

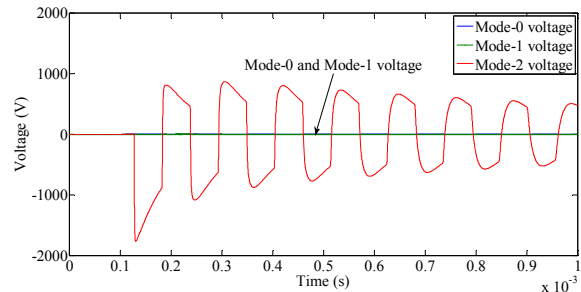


Fig. 7. Mode-0, mode-1, and mode-2 voltages calculated from simulation results of voltages at the receiving end of the circuit in Fig. 1(b).

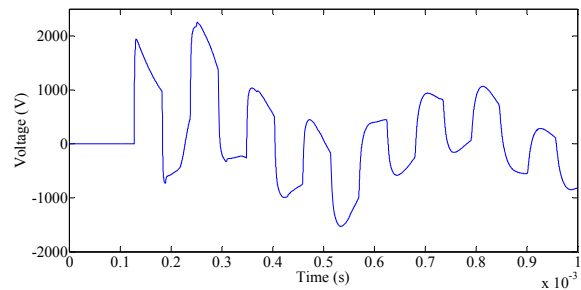


Fig. 8. Simulated sheath-a receiving end voltage in the circuit of Fig. 1(b) with the source grounded.

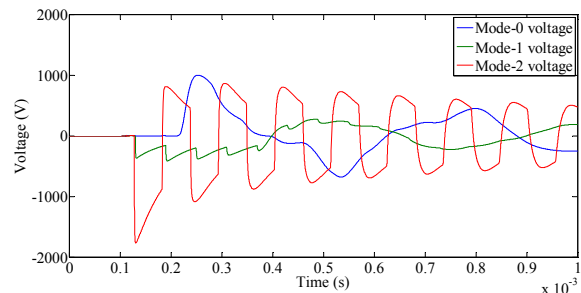


Fig. 9. Mode-0, mode-1 and mode-2 voltages calculated from simulation results of voltages at the receiving end of the circuit in Fig. 1(b) with the source grounded.

IV. TRANSIENTS ON A CROSS-BONDED CABLE

Crossbonding of metallic sheaths is a technique used in long high-voltage AC cables to reduce losses due to induced sheath currents and improve power transmission capacity. It consists of a regular transposition of the metallic sheaths, analogous to the transposition of phases in overhead power lines. A crossbonding point causes refraction/reflection of a travelling wave on the cable system resulting in higher sheath overvoltage [8, 10-13, 21]. An accurate transient simulation must therefore account for the crossbonding of sheaths.

The most straightforward model for a crossbonded cable represents each minor section separately (discrete model). This gives an accurate time-domain solution and allows the inclusion of a lead wire impedance. On the other hand the simulation of long cables becomes tedious and time consuming.

If the impedance of the lead wire is neglected, the rotation of sheaths may be included in the per-unit-length parameters of the cable, allowing to represent a major section with 3 cross-bonded segments using a single model. Though this is accurate in steady-state, it neglects the reflection/refraction phenomena observed during a transient.

Cross-bonded cables usually have the sheaths short-circuited and grounded at each major section to reduce sheath overvoltages, as shown in Fig. 10. In this case, the three-phase sheath may be considered as a single conductor thus reducing the total number of conductors from 6 to 4.

The so-called homogeneous model of a cross-bonded cable with the sheaths grounded includes the effect of cross-bonding in the per-unit-length parameters and uses a single equivalent sheath [11, 22]. This model has a positive impact on the simulation time by reducing the number of cable sections by a factor of 3 and by reducing a 6th order system to a 4th order one. A 3rd order model is possible if we assume the voltage in the sheath is continuously zero. The homogeneous model also makes possible the computation of the propagation characteristics of cross-bonded systems [11, 22].

In Section A the theory for the homogeneous model is explained and the modes of propagation in a cross-bonded cable are computed. Transients in one and in two major sections are presented in sections B and C, respectively.

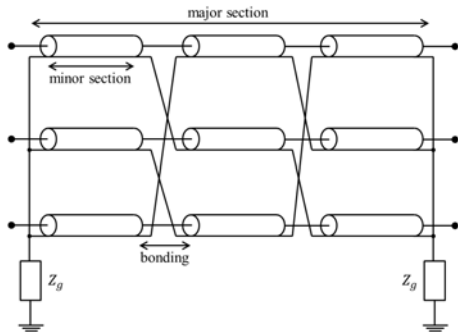


Fig. 10. Major section of a cross-bonded cable system with sheaths grounded.

A. Homogeneous model of a cross-bonded cable

A cross-bonded cable which sheaths are grounded at each

major section can be approximately represented by an equivalent homogeneous cable composed of three core conductors and one metallic sheath [11, 13, 14, 21]. The construction of a homogeneous model is explained as follows. Consider \mathbf{Z} and \mathbf{Y} the impedance and admittance matrices of a minor section of the cable

$$\mathbf{Z} = \begin{bmatrix} \mathbf{Z}_{cc} & \mathbf{Z}_{cs} \\ \mathbf{Z}_{cs}^T & \mathbf{Z}_{ss} \end{bmatrix} \quad \mathbf{Y} = \begin{bmatrix} \mathbf{Y}_{cc} & \mathbf{Y}_{cs} \\ \mathbf{Y}_{cs}^T & \mathbf{Y}_{ss} \end{bmatrix} \quad (10)$$

where subscript 'cc' is used for impedance/admittance matrices between cores, 'ss' for sheath impedance/admittance matrices and 'cs' for core-to-sheath impedance/admittance matrices. The first step in the construction of a homogeneous model is to account for the rotation of voltages and currents in metallic sheaths. This is done using a rotation matrix \mathbf{R} as follows

$$\mathbf{Z}' = \frac{1}{3} \{ \mathbf{R}^T \mathbf{Z} \mathbf{R} - \mathbf{R} \mathbf{Z} \mathbf{R}^T - \mathbf{Z} \} = \begin{bmatrix} \mathbf{Z}'_{cc} & \mathbf{Z}'_{cs} \\ \mathbf{Z}'_{cs}^T & \mathbf{Z}'_{ss} \end{bmatrix} \quad (11)$$

$$\mathbf{Y}' = \frac{1}{3} \{ \mathbf{R}^T \mathbf{Y} \mathbf{R} - \mathbf{R} \mathbf{Y} \mathbf{R}^T - \mathbf{Y} \} = \begin{bmatrix} \mathbf{Y}'_{cc} & \mathbf{Y}'_{cs} \\ \mathbf{Y}'_{cs}^T & \mathbf{Y}'_{ss} \end{bmatrix} \quad (12)$$

$$\mathbf{R} = \begin{bmatrix} \mathbf{U} & \mathbf{0} \\ \mathbf{0} & \mathbf{R}_{33} \end{bmatrix} \quad \mathbf{R}_{33} = \begin{bmatrix} 0 & 0 & 1 \\ 1 & 0 & 0 \\ 0 & 1 & 0 \end{bmatrix} \quad (13)$$

Where \mathbf{U} is an identity matrix and $\mathbf{0}$ is a null matrix, both 3-by-3. Developing the products in (11) gives the following impedance sub-matrices

$$\mathbf{Z}'_{cc} = \mathbf{Z}_{cc} \quad (14)$$

$$\mathbf{Z}'_{cs} = \{ \mathbf{Z}_{cs} \mathbf{R}_{33} + \mathbf{Z}_{cs} \mathbf{R}_{33}^T + \mathbf{Z}_{cs} \} / 3 \quad (15)$$

$$\mathbf{Z}'_{ss} = \{ \mathbf{R}_{33}^T \mathbf{Z}_{ss} \mathbf{R}_{33} + \mathbf{R}_{33} \mathbf{Z}_{ss} \mathbf{R}_{33}^T + \mathbf{Z}_{ss} \} / 3 \quad (16)$$

For the core-sheath matrix \mathbf{Z}'_{cs} , each element of a row is equal to the average of the same row of \mathbf{Z}_{cs} . This is easily seen from

$$\mathbf{Z}'_{cs} = \frac{1}{3} \mathbf{Z}_{cs} \{ \mathbf{R}_{33} + \mathbf{R}_{33}^T + \mathbf{U} \} = \frac{1}{3} \mathbf{Z}_{cs} \begin{bmatrix} 1 & 1 & 1 \\ 1 & 1 & 1 \\ 1 & 1 & 1 \end{bmatrix} \quad (17)$$

For the self-sheath impedance, multiplication by \mathbf{R}_{33} will rotate the rows and columns of \mathbf{Z}_{ss} such that a diagonal element of \mathbf{Z}'_{ss} becomes the average of the diagonal elements of \mathbf{Z}_{ss} and an off-diagonal element of \mathbf{Z}'_{ss} becomes the average of the off-diagonal elements of \mathbf{Z}_{ss}

$$Z'_{sss} = \frac{1}{3} \sum_{i=1}^3 (Z_{ss})_{ii} \quad (18)$$

$$Z'_{ssm} = \frac{1}{3} \sum_{i=1}^2 \sum_{j=i+1}^3 (Z_{ss})_{ij} \quad (19)$$

From the similarity between equations (11) and (12), it is clear that the admittance submatrices in (12) follow the reasoning explained above.

There is no approximation in deriving the matrices \mathbf{Z}' and \mathbf{Y}' of a crossbonded cable except the assumption that all minor sections have the same length. Therefore the approach is exact in steady-states, i.e. in a frequency domain. The same cannot

be directly applied to transients since the reflected/refracted waves originated at cross-bonding points are not represented in \mathbf{Z}' and \mathbf{Y}' .

The sheaths being short-circuited and grounded at each major section allows a further simplification of the problem as the three sheaths are reduced to a single conductor. This way, the impedance and admittance matrices become 4-by-4

$$\mathbf{Z}'' = (\mathbf{T}\mathbf{Z}'^{-1}\mathbf{T}^T)^{-1} \quad (20)$$

$$\mathbf{Y}'' = \mathbf{T}\mathbf{Y}'\mathbf{T}^T \quad (21)$$

$$\mathbf{T} = \begin{bmatrix} 1 & 0 & 0 & 0 & 0 & 0 \\ 0 & 1 & 0 & 0 & 0 & 0 \\ 0 & 0 & 1 & 0 & 0 & 0 \\ 0 & 0 & 0 & 1 & 1 & 1 \end{bmatrix} \quad (22)$$

Fig. 11 shows frequency responses of modal attenuations and propagation velocities calculated from the homogeneous model of a cross-bonded cable with the cross-section in Fig. 2. Comparing Figs. 11 and 3, with the propagation characteristics of a cross-bonded cable and a normal-bonded cable, respectively, it is observed that a cross-bonded cable has 4 propagation modes whereas a normal-bonded cable has 6. There exists no difference for mode 0 (earth-return mode) between Fig. 3 and Fig. 11. Also, no significant differences are observed for the coaxial modes (modes 3 to 5 in Fig. 3 and mode 3 in Fig. 11), except that the normal-bonded cable has 3 coaxial modes whereas the cross-bonded cable has only one. This is because, the cross-bonded cable having only one sheath, there is only one mode with return through the sheath in the same way as there is only one earth-return mode in any transmission system. It is also observed that modes 1 and 2 in a normal-bonded cable (intersheath modes) still exist in a cross-bonded cable but they have a different velocity in the cross-bonded cable. Actually, what is usually called intersheath mode is in fact an interphase mode and in a cross-bonded cable this mode propagates between cores rather than between sheaths.

B. Simulation of one major section ($x=6$ km)

Consider a major section having a total length of 6 km divided into 3 equal minor sections and having the cross-section of Fig. 2. At both ends of the major section, the three-phase sheaths are short-circuited with a grounding resistance $R_g = 10 \Omega$. A 1.2 $\mu\text{s}/50 \mu\text{s}$ voltage impulse with 2 kV is applied to core-a.

Fig. 12 shows EMTP simulation results for the core-a receiving end voltage using a discrete cable model (each minor section modeled separately) and a homogeneous model. It is observed that the voltage waveform of the homogeneous model is much smoother and the maximum overvoltage is higher than in the discrete model. It is also noted that travelling waves initially arrive at the same time for the two models, but as time goes by, the moments of arrival of a wave are no longer simultaneous. This is because in the first moments of simulation there is still no wave reflected from a

cross-bonding point arriving at the receiving end. When this happens, the two voltage waveforms start to diverge more because the discontinuity caused by cross-bonded points is not represented in the homogeneous model.

C. Simulation of two major sections ($x=12$ km)

Consider two major sections having a total length of 12 km, divided into 6 equal minor sections with the cross-section as in Fig. 2. At both ends of each major section, the three-phase sheaths are short-circuited with a grounding resistance $R_g = 10 \Omega$. A 1.2 $\mu\text{s}/50 \mu\text{s}$ voltage impulse with 2 kV is applied to core-a.

Fig. 13 shows EMTP simulation results for the core-a receiving end voltage using a discrete cable model (each minor section modeled separately) and a homogeneous model. By comparison of Figs. 12 and 13 it is observed that the two models agree more as the length of the system and the number of grounding points increase. This is because reflected/refracted waves are attenuated when passing through a grounding point and when travelling a longer distance in the cable. Therefore, the difference becomes less important between a discrete model and a homogeneous model which does not represent these reflected/refracted waves.

V. CONCLUSION

This paper presents a study of intersheath modes in 3-phase single-core coaxial cables. Circuits for intersheath mode energization are explained and investigated based on EMTP simulations and on the propagation characteristics of the cable. It is observed that when a source is grounded (approach used often in field tests to avoid dangerous overvoltages) various modal components (voltages and currents) are produced and it becomes difficult to observe the intersheath modes. A so-called homogeneous model for long cross-bonded cables is explained and its performance is demonstrated with transient simulations in EMTP. A homogeneous model accounts for the transposition of sheaths at cross-bonding points and for the grounding of sheaths at major sections. The homogeneous model has benefits in terms of simulation time: (1) a major section cable modeled as a whole instead of having a separate model for each minor section, reducing the number of cable models in a simulation by a factor of 3; (2) the grounded sheaths can be considered as a single conductor instead of three. Therefore, the homogeneous model has order 4 instead of 6 (4 conductors, 4-by-4 per-unit-length matrices). This further reduces to 2/3 the number of equations to solve in the simulation of each cross-bonded cable. The homogeneous model has another advantage of allowing the computation of propagation characteristics of a cross-bonded cable. The homogeneous model is highly accurate in steady-state, i.e. in frequency domain, but it is less accurate for simulating transients as it does not represent the reflected/refracted waves produced at cross-bonding points. Nevertheless, simulations show that as the length and the number of sheath groundings increase, the accuracy of the homogeneous model is improved

with results approaching those of a discrete cable model.

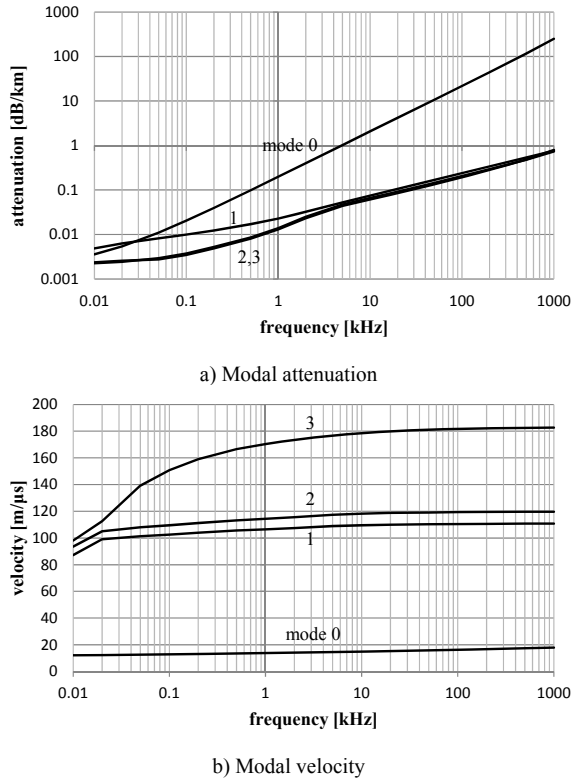


Fig. 11. Modal propagation on the homogeneous model of a cross-bonded cable corresponding to Figs. 10 and 2.

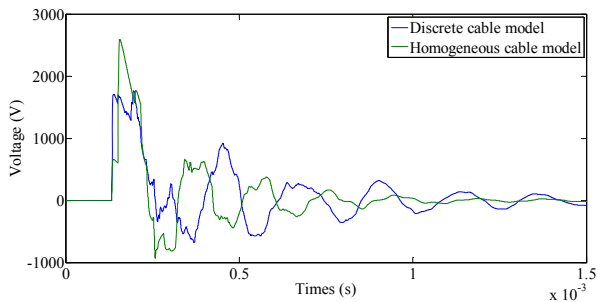


Fig. 12. Core-a receiving end voltage in a cross-bonded cable having a single major section. Results computed using a discrete and a homogeneous cable model.

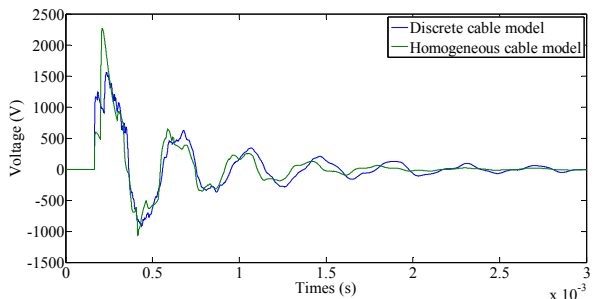


Fig. 13. Core-a receiving end voltage in a cross-bonded cable having 2 major sections. Results computed using a discrete and a homogeneous cable model.

REFERENCES

[1] C. W. G. C4.502, "Power System Technical Performance Issues Related to the Application of Long HVAC Cables," in CIGRE Technical Brochure TB556, Oct. 2013.

[2] L. Colla, M. Robolini, and F. Iliceto, "400kV AC new submarine cable links between Sicily and the Italian mainland," presented at the CIGRE Session C4-116, Paris, 2008.

[3] Energinet, Cable Action Plan: 132-150kV Grids, www.energinet.dk, March 2009.

[4] L. M. Wedepohl and D. J. Wilcox, "Transient analysis of underground power transmission systems: system model and wave propagation characteristics," Proc. IEE, vol. 120, 1973.

[5] L. M. Wedepohl and D. J. Wilcox, "Estimation of transient sheath overvoltages in power-cable transmission systems," Electrical Engineers, Proceedings of the Institution of, vol. 120, pp. 877-882, 1973.

[6] L. M. Wedepohl and C. S. Indulkar, "Switching overvoltages in short crossbonded cable systems using the Fourier Transform," Proc. IEE, vol. 122, pp. 1217-1221, 1975.

[7] R. G. Wasley and S. Selvavinayamoorthy, "Computation of sheath transient response in single-point bonded cable section," IEEE Trans. Power App. & Syst., vol. PAS-96, pp. 248-254, 1977.

[8] D. J. Wilcox, "Transient phenomena in crossbonded cable systems ; analytical results," Proc. IEE, vol. 125, pp. 999-1005, 1978.

[9] A. Ametani, "Wave Propagation Characteristics of Cables," IEEE Transactions on Power Apparatus and Systems, vol. PAS-99, pp. 499-505, 1980.

[10] W. D. Humpage, K. P. Wong, and T. T. Nguyen, "Z-transform electromagnetic transient analysis of crossbonded cable transmission systems," Proc. IEE, vol. 128, pp. 55-62, 1981.

[11] N. Nagaoka and A. Ametani, "Transient calculations on crossbonded cables," IEEE Trans. Power Apparatus and Systems, vol. 102, pp. 779-787, 1983.

[12] N. Nagaoka, M. Yamamoto, and A. Ametani, "Surge propagation characteristics of a POF cable," Electrical Engineering in Japan, vol. 105, pp. 67-75, 1985.

[13] Y. Itoh, N. Nagaoka, and A. Ametani, "Transient analysis of a crossbonded cable system underneath a bridge," IEEE Trans. Power Delivery, vol. 5, pp. 527-532, 1990.

[14] A. Ametani, Distributed-Parameter Circuit Theory. Tokyo: Corona Pub.Co., 1990.

[15] A. Ametani and C. T. Wan, "Sheath overvoltages due to faults on an EHV cable," in International Conference on Power System Transients (IPST 95), Sep. 1995, pp. 87-92.

[16] A. Ametani, Y. Miyamoto, and N. Nagaoka, "Semiconducting layer impedance and its effect on cable wave-propagation and transient characteristics," IEEE Trans. Power Delivery, vol. 19, pp. 1523-1531, 2004.

[17] U. S. Gudmundsdottir, "Modeling of Long High Voltage AC Cables in Transmission Systems," Ph.D. Thesis, Aalborg University, 2010.

[18] U. S. Gudmundsdottir, "Proximity Effect in Fast Transient Simulations of an Underground Transmission Cable", EPSR, vol. 115, pp. 50-56, October 2014.

[19] T. Ohno, C. L. Bak, A. Ametani, W. Wiechowski, and T. K. Sorensen, "Statistical distribution of energization overvoltages of EHV cables," IEEE Trans. Power Delivery, vol. 28, pp. 1423-1432, 2013.

[20] J. Mahseredjian, S. Denetiere, L. Dubé, B. Khodabakhchian and L. Gérin-Lajoie, "On a new approach for the simulation of transients in power systems", Electric Power Systems Research, Vol. 77, Issue 11, September 2007, pp. 1514-1520.

[21] N. Nagaoka et al., "Transient sheath voltage characteristic of a crossbonded cable installed within a tunnel", Transactions IEE Japan, vol. 111-B (7), pp. 784-790, 1985.

[22] A. Ametani, Y. Miyamoto and N. Nagaoka, "An investigation of a wave propagation characteristic on a cross-bonded cable," IEE Japan Trans., vol. Vol. 123-B, pp. 395-401, 2003.